Journal of Atmospheric and Solar–Terrestrial Physics 281 (2026) 106780

Contents lists available at ScienceDirect

Journal of Atmospheric and Solar–Terrestrial Physics

journal homepage: www.elsevier.com/locate/jastp

Research paper

Impact of severe geomagnetic storm on atmospheric electric field over the Arctic region during May 2024

Kavita [a], Saurabh Das [a,*], Nuncio Murukesh [b]

[a] Department of Astronomy, Astrophysics and Space Engineering, Indian Institute of Technology Indore, Simrol, Indore, 453552, Madhya Pradesh, India
[b] National Centre for Polar and Ocean Research (NCPOR), Headland Sada, 403804, Goa, India

ARTICLE INFO

Dataset link: http://omniweb.gsfc.nasa.gov, https://cosmicrays.oulu.fi/, https://superdarn.ca/, https://ccmc.gsfc.nasa.gov/, https://space.fmi.fi/image/www/index.php?, https://data.ncpor.res.in/newhtml/3

Keywords:
Arctic
Atmospheric electric field
Geomagnetic storm

ABSTRACT

During May 10–11, 2024, a series of intense solar eruptions caused one of the most significant geomagnetic storms in recent history. This study investigates the impact of this severe Geomagnetic storm on temporal variations in the atmospheric electric field over the Arctic region. The Electric field measurements were obtained at Ny-Ålesund (78.9° N, 11.9° E), Norway in the Arctic Circle. The study reveals a complex interaction between space weather, ionosphere and atmospheric electricity through three key processes: forbush decrease (FD), ground-level enhancement (GLE) and Dawn–Dusk potential. A decrease in the vertical atmospheric electric field (E_z) during a FD was observed. This may be due to the decrease in current density (j_z) alongside less ionization by reduced cosmic rays into the Earth's atmosphere during the shock and complex ejecta associated with the storm. In contrast, GLE event were recorded during the storm's recovery phase, leading to an increase in E_z. Additionally, the downward mapping of horizontal electric fields significantly contributes to variations in E_z.

1. Introduction

The Earth's atmosphere is highly intricate and electrically dynamic, with charges moving between the surface and the ionosphere. The vertical atmospheric electric field (E_z) is present because of the potential difference between these two regions. Wilson (1921) proposed the idea of the global electrical circuit (GEC), suggesting that the Earth functions as a leaky capacitor with thunderstorms acting as a global generator of atmospheric electricity. In addition to thunderstorms, other atmospheric processes, such as aerosol concentrations, cloud cover, and precipitation events, also contribute to the GEC (Potdar and Siingh, 2024). The E_z is the main element of the GEC and also serves as a critical tool for understanding the coupling between space weather and near-surface electrical environments, particularly in the high-latitude regions. This coupling allows ionospheric potentials to influence the E_z and air-Earth current (j_z) measured at the ground (Michnowski et al., 2021). The E_z is present even in fair-weather conditions and typically varies between +100 to +200 V/m (Marshall et al., 1999; Rycroft et al., 2008; Li et al., 2025).

Space weather events, such as solar flares, coronal mass ejections (CMEs), interplanetary shocks, solar energetic particles (SEP), and galactic cosmic rays (GCRs), can change the ionization of the Earth's upper atmosphere and influence the GEC by modifying the parameters like atmospheric conductivity, the flow of vertical currents, electric potential, and the state of the ionosphere (Siingh and Singh, 2010). In addition, when GCRs penetrate into the atmosphere, they can affect nucleation and aerosol formation through ionization (Shumilov et al., 2015). GCRs are energetic particles primarily consisting of protons, as well as heavier atomic nuclei and electrons (Blasi, 2013). When GCRs have energies typically exceeding 500 MeV, they can penetrate deep into the atmosphere and collide with atmospheric atoms, producing secondary particles such as neutrons, muons, and electrons. This leads to a sudden increase in cosmic ray intensity (CRI) at the surface, which can be detected by ground-based detectors like neutron monitors. Such events, characterized by a rapid and significant rise in neutron monitor counts are known as Ground Level Enhancements (GLEs) (Souvatzoglou et al., 2014; Crosby et al., 2024) which can cause significant variations in E_z. Conversely, a sudden reduction in CRI, known as a Forbush decrease (FD), can occur due to enhanced magnetic fields in the sheath and ejecta regions of an Interplanetary coronal mass ejections (ICME). FDs typically reduce GCR flux by about 3%–20% and recover gradually over several hours to a few days (Chauhan et al., 2008). These decreases can also lead to measurable variations in E_z.

Li et al. (2024) examined the E_z behavior using observations from eight stations across low and mid latitudes during the major geomagnetic storm of April 2023, which revealed anomalous behavior in E_z.

* Corresponding author.
E-mail addresses: kavitapnp97@gmail.com (Kavita), saurabh.das@iiti.ac.in (S. Das), nuncio@ncpor.res.in (N. Murukesh).

https://doi.org/10.1016/j.jastp.2026.106780
Received 1 January 2026; Received in revised form 18 February 2026; Accepted 3 March 2026
Available online 7 March 2026

Among these stations, five exhibited an increase in E_z by approximately 62.5%, while the remaining three stations, which were located near each other, showed a decrease in E_z values. The variability in E_z at different stations arises from differences in ionospheric electric potential across latitudes and longitudes, which creates horizontal potential gradient. These gradients modify the j_z differently at different locations, leading to contrasting E_z responses even during the same storm. Additionally, Li et al. (2023) reported a decrease in E_z at two mid-latitude stations coinciding with a reduction in CRI. They suggested that CME-associated shocks and magnetic clouds (MCs) impede incoming GCRs, thereby reducing the electric potential of ionosphere and consequently, the current, leading to a reduction in the E_z. In contrast, some studies like Engfer and Tinsley (1999) did not observe any significant change in E_z, whereas Smirnov (2014), Tacza et al. (2022) have found an increase in E_z during the FD. Fu et al. (2025) also observed an increase in E_z during the FD phase and a decrease during the GLE phase at mid-latitude Gar station of China during the May 2024 geomagnetic storm and explained this behavior assuming constant ionospheric potential.

On the other hand, various studies have shown that during GLEs, also the response of E_z is not uniform, with both increases and decreases reported. Tonev (2024) reported increases in both E_z and j_z during strong Solar proton event (SPE) accompanied by GLEs. The study explains that the increase in E_z is due to conductivity reductions caused by aerosol formation and the injection of positive charges into the polar atmosphere. However, other studies like Michnowski et al. (2014) have observed decreases in E_z during GLEs, particularly at mid-latitude stations. Tacza et al. (2018) reported the decrease in electric field values at two low-latitude stations which can be attributed to an increase in local ground ionization due to enhanced secondary high-energy particle fluxes. These particles increase atmospheric conductivity, and according to Ohm's law, under the assumption of a constant j_z, there is a decrease in the E_z. Similar decreases in the electric field have been observed in balloon measurements during SPE event accompanied by a GLE (Holzworth et al., 1987; Reagan et al., 1983). Consistent with these findings, Mallios et al. (2022) also reported that GLE events significantly increase atmospheric ionization, leading to enhanced electrical conductivity and reduced columnar resistance under fair-weather conditions. These contrasting responses indicate that the sign and magnitude of the E_z variation during GLEs depend on the combined effects of enhanced ionization, conductivity changes, modifications of columnar resistance, weather conditions, and possible changes in the ionospheric potential. The influence of these mechanisms likely varies with latitude, atmospheric conditions, and the characteristics of the SEP event, leading to either an increase or a decrease in E_z.

Studying the GEC in the polar regions presents additional challenges as solar wind-magnetosphere interactions drive continuous plasma circulation over the polar region. This large-scale plasma and magnetic field circulation extends down to the ionosphere, resulting in a two-cell convection pattern (Papitashvili et al., 1994; Kumar et al., 2009). Plasma flow in the presence of a magnetic field induces an electric field perpendicular to the flow direction, creating electric potentials across the polar cap. This is not uniform, resulting in strong dawn–dusk electric potentials across the polar ionosphere. These horizontal ionospheric potential differences penetrate the lower atmosphere, superimposing on the global diurnal electric potential, and lead to observable variations in E_z and j_z at the ground (Reddell et al., 2004; Park, 1976; Roble and Hays, 1979).

Victor et al. (2015) reported a significant enhancement of the surface electric field at Antarctica, during the geomagnetic storm of 25–26 January 2006. This enhancement was observed with an increase in the dawn–dusk potential and occurred when the station was located within the auroral oval. Kleimenova et al. (2011, 2013, 2018) analyzed the variation of E_z at the Arctic during the substorm and showed that E_z exhibited an increase and decrease in value during the local morning and evening, respectively. This deviation depends on the station's position with respect to the positive and negative vortex of the polar ionospheric plasma convection. Kleimenova et al. (2013, 2017) have also shown that disturbances in the X-component of the magnetic field were accompanied by the corresponding changes in E_z. Although no clear relationship between the magnitude of E_z and the magnetic field was observed.

While several studies have explored the impact of geomagnetic storms on E_z, their findings are often inconsistent. In the present study, the impact of a severe geomagnetic storm on the E_z at high latitudes, the Arctic region, is investigated. This geomagnetic storm has provided an opportunity to study the interaction between the magnetosphere and atmosphere by focusing on three significant phenomena, including the FD, GLE, and the horizontal mapping of the electric field affecting the E_z. During this event, the complex interactions between the solar activity, cosmic ray intensity, horizontal mapping of the electric field, and the atmospheric electric field were observed.

2. Study site and data

Measurements of the near-surface E_z have been conducted at the Gruvebadet Lab, Himadri Research Station located at the Ny-Ålesund (78.9° N, 11.9° E) region of Svalbard, Norway, Arctic. The E_z is measured using an electric field monitor (EFM-100, Boltek) with a response time of 0.1 s. It records twenty readings per second within a measurement range of ±20 kV/m and a resolution of 0.01 kV/m. Meteorological parameters were collected from the Norwegian Center for Climate Services (NCCS) as well as from various ground instruments to understand the atmospheric conditions at Arctic location. For precipitation measurement, the Particle Size and Velocity (ParSiVEl^2) optical disdrometer (OTT Hydromet GmbH) was used. A Ceilometer (CL51, Vaisala), based on Light Detection and Ranging (LIDAR) technology, was used to measure cloud base height (CBH). Wind speed, relative humidity and temperature data were obtained from the European Centre for Medium-Range Weather Forecasts (ECMWF) reanalysis v5 (ERA5).

The data for space weather parameters like the interplanetary magnetic field (IMF), the north–south component of the IMF (B_z), solar wind speed (V), proton temperature (Temp), and symmetric component of the ring current index (SYM-H) are taken from NASA's OMNIweb. The variations of the X component of the magnetic field were analyzed using data from three stations NAL (78.92° N, 11.95° E), LYR (78.2° N, 15.8° E), and HOR (77.00° N, 15.60° E) of the Scandinavian magnetometer chain IMAGE to identify geomagnetic disturbances and magnetic bays and compared with simultaneous E_z measurements. In addition, CRI data were obtained from the OULU neutron monitor located in Finland. It has an effective vertical cutoff rigidity of approximately 0.8 GV, and the data were analyzed at a temporal resolution of 1 min. Super Dual Auroral Radar Network (SuperDARN) data and Weimer model are used to study ionospheric convection and to quantify large-scale plasma convection and dawn–dusk electric potential variations during the storm.

3. Methodology

To study the impact of geomagnetic storms on the E_z, the identification of the perturbed electric field segment is critical. Since there also exists natural variability in the electric field, the following two statistical techniques have been used for this purpose.

3.1. Criteria and identification of fair-weather condition

The atmospheric electric field is widely known to be affected by the local meteorological conditions, including cloud cover, precipitation, humidity, wind, and other factors such as aerosol concentration and topography. To accurately assess the impact of geomagnetic storms on the E_z, it is essential to understand these meteorological influences.

Defining fair-weather conditions is very important and necessary, as they are highly subjective from place to place. Several studies have already defined the fair-weather condition. Harrison and Nicoll (2018) defined fair-weather days as those free from any type of hydrometeors, no clouds with bases below 1500 m, and surface wind speeds between 1 m/s and 8 m/s. Kleimenova et al. (2011) defined the fair-weather conditions for Hornsund station (Arctic) as days without any strong winds, precipitation, fog, or low-level cloud cover and negative E_z values. Siingh et al. (2013) selected fair-weather days for Maitri station (Antarctica) based on wind speeds less than 10 m/s. For the present study, fair-weather days are defined as (1) no hydrometeors such as rain and snow; (2) wind speed less than 8 m/s; and (3) no low level cloud.

3.2. Statistical detection using Bayesian blocks and HOP method

In addition to the traditional method of comparing E_z with fair-weather days, a combination of the Bayesian Blocks (BB) and HOP method (Meyer et al., 2019) was applied to detect deviations in E_z. The 1-minute average value of E_z and one standard deviation value were taken. The BB method divides the E_z time series into contiguous blocks, within which the electric field remains statistically constant until a significant change occurs. These change points are the boundaries between these blocks, which are determined using Bayesian analysis, with a significance level of 0.05 applied to control the number of segments. If a new data point falls within this significance level, then it is included in the existing block; otherwise, a change point is identified, indicating a shift in the electric field. This approach provides a precise analysis of short-term variations in E_z. The mean value serves as a reference, representing the average electric field value over the entire dataset to compare BB segmentations and identify significant deviations. After the BB segmentation, the HOP method was used to find notable changes in E_z (Eisenstein and Hut, 1998). The method segregates the time series into multiple groups based on when the BB values are significantly below the mean value.

4. Results

4.1. Description of the event of Mother's Day storm

Mother's Day geomagnetic storm during 10–11 May, 2024 impacts the Earth's magnetic field with a series of solar flares and overlapping multiple CMEs rather than a single fast CME. This disturbance led to enhanced auroral displays in both hemispheres and was recorded as the most intense storm since 1989 (Hayakawa et al., 2025). A solar active region (AR3664) on May 8–9, 2024, produced multiple X-class solar flares and CMEs. The Earth's magnetosphere was compressed by the passage of CME and sheaths of CME-driven shocks, which were the primary cause of geomagnetic storms (Gonzalez-Esparza et al., 2024).

Space weather parameters from 12:00 UTC on May 10 to 12:00 UTC on May 11 are shown in Fig. 1 with a 1-minute temporal resolution. The different phases of the geomagnetic storm, including storm onset, main phase, and recovery phase, are characterized using the temporal variations of the SYM-H. The negative values of SYM-H indicate an intensification of a ring current, resulting in a temporary weakening of Earth's magnetic field. At 16:34 UTC on May 10, the ICME reached the L1-point, as recorded by the DSCOVR spacecraft (Tulasiram et al., 2024). Shortly after, 31 min later, at 17:05 UTC, the sudden storm commencement (SSC) was observed as a sudden increase in the IMF, solar wind speed, and proton temperature. This marks the arrival of a shock associated with ICME impacting Earth and plays a key role in accelerating the SEP. This event is indicated by the first red line in Fig. 1. This time lag of 31 min is because of the time ICME takes to travel from the L1 point to Earth's bow shock. The IMF value reaches 22 nT, and solar wind speed increases from 443 km/s to 714 km/s, proton temperature from 4.51×10^4 K to 91.8×10^4 K, while the (B_z) component of the IMF drops to −15 nT, indicating a southward turning of B_z. This southward orientation is an important driver of geomagnetic storms, as it enhances magnetic reconnection with Earth's magnetosphere, leading to increased geomagnetic activity. At the same time, the SYM-H suddenly increased to 88 nT due to the compression of the dayside magnetosphere and an increase in magnetopause current, indicating the initial phase of the geomagnetic disturbances. Following this, the SYM-H began to decrease, signifying strong ring current intensification and the onset of the storm's main phase (Araki, 1977; Tulasiram et al., 2024).

A shock is followed by a sheath region, characterized by a turbulent magnetic field and hot, dense plasma (Burlaga et al., 1981). In Fig. 1, the sheath region is indicated between the two red dashed lines, marked by enhanced fluctuations in the magnetic field. After the sheath region, the proton temperature exhibits multiple dips, and the magnetic field strength peaks at approximately 70 nT. These signatures, including temperature reduction and enhanced magnetic field, are the key characteristics of complex ejecta resulting from the interaction of multiple CMEs (Burlaga et al., 2002). Supporting this, Liu et al. (2024) also reported the occurrence of two complex ejecta during the May 2024 geomagnetic storm.

The passage of the shock-sheath structure followed by the complex ejecta caused a clear FD, marked by a rapid reduction in CRI as shown in Fig. 1(f). This decline was also observed simultaneously by multiple ground-based neutron monitors worldwide. In Fig. 1(f), the FD onset began with the initial decrease in CRI and reached its maximum depth at 23:26 UTC on May 10, 2024. Subsequently, a GLE event occurred, with an onset around 01:30 UTC and a peak around 03:00 UTC on May 11. This event has been recorded as GLE#74 in the GLE dataset (Hayakawa et al., 2025). The main phase of the storm lasted 9 h and is observed as three significant drops in the SYM-H, recorded as −183 nT at 19:21 UTC on May 10, followed by a deeper drop to −354 nT at 23:12 UTC the same day, and reaching a minimum of −518 nT at 02:14 UTC on May 11 (Fig. 1(e)), making it the most intense geomagnetic storm in recent history (Hajra et al., 2024).

4.2. Detection of significant changes in electric field

In Fig. 2(a), E_z values are compared to the inter-quartile range (25th–75th percentile) of fair-weather E_z values, computed for each minute of the day. For long-term fair-weather conditions, data between July 2023 to December 2024 were examined, during which only 44 fair-weather days were recorded. It is to be noted that the number of fair-weather days over the Arctic region was limited, typically only 3–4 days per month (Kleimenova et al., 2018). The fair-weather day's mean is 126 V/m, and the 25th and 75th percentile values of E_z from fair-weather days were used as lower and upper quartiles, shown as a shaded gray region. A rolling average with a window of 1200 data points (1 min) was applied to smooth out rapid fluctuations, represented by a black line.

On May 10, in the beginning, the E_z remains relatively stable, with fluctuation ranging around 50 V/m, indicating a typical fair-weather condition. Around 17:05 UTC, a small deviation in E_z from fair-weather values is observed, followed by a rapid recovery. Around 20:00 UTC, it starts to decrease slowly but remains within the fair-weather conditions. Later, a noticeable decrease in the E_z values begins around 22:55 UTC on May 10, and reaches a minimum value of −44.13 V/m around 23:30 UTC. Following the dip, an increase in E_z values was observed around 01:30 UTC on May 11, exceeding fair-weather conditions. After a gradual decline, a second, more prominent enhancement around 05:30 UTC can be seen with E_z values reaching as high as 200–300 V/m.

The BB and HOP algorithms were applied to the E_z data to analyze these variations further and identify statistically significant dips as shown in Fig. 2(b). The black dots show 1-minute average E_z values along with their standard deviation values. The horizontal red line

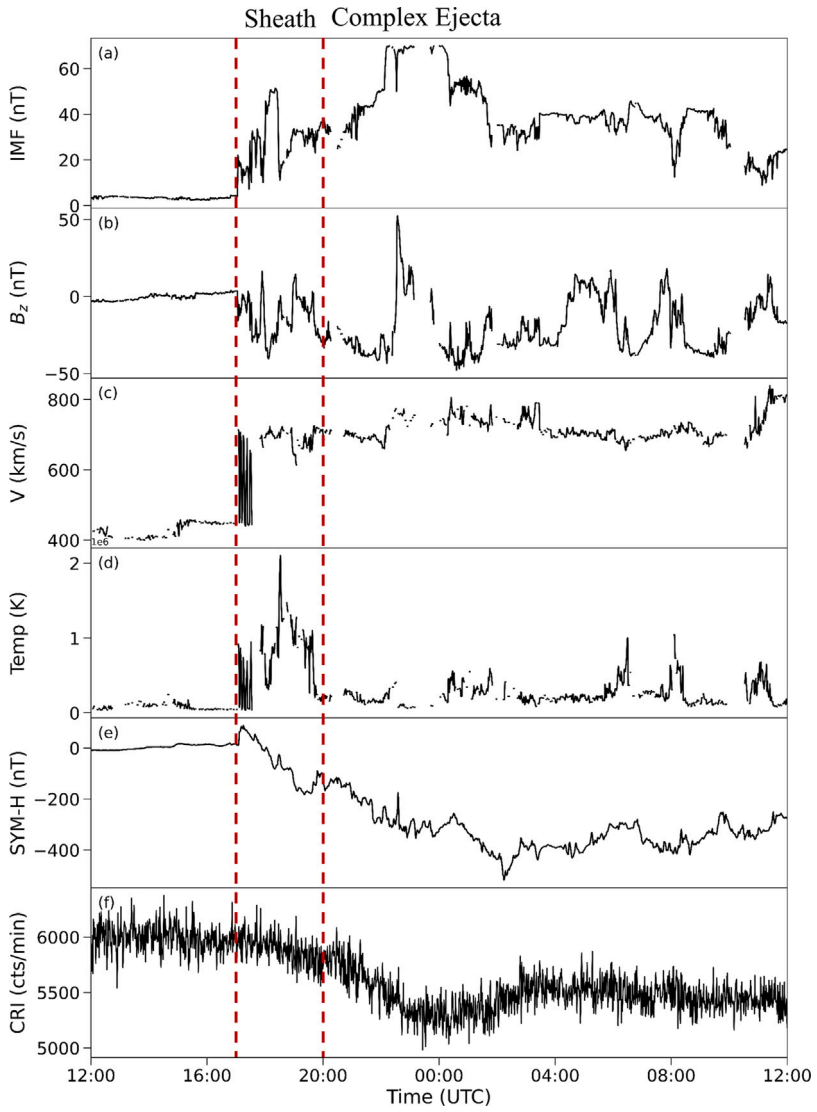

Fig. 1. Temporal variations of key space weather parameters influencing Earth's magnetosphere, including (a) the interplanetary magnetic field (IMF), (b) north–south component of IMF (B_z), (c) solar wind speed (V), (d) proton temperature (Temp), (g) SYM-H, (f) Cosmic Ray Intensity (CRI).

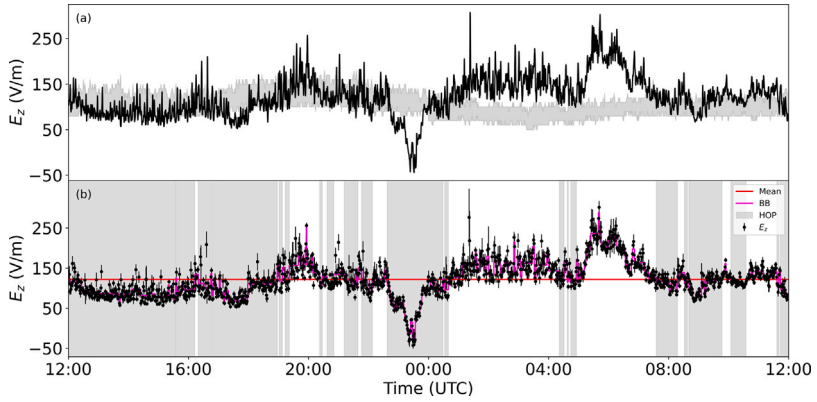

Fig. 2. Temporal variation of the E_z during May 10–11, 2024, presented using two approaches: (a) comparison with fair-weather conditions, (b) a combination of the BB and HOP algorithms to detect significant deviations.

is the mean value of the dataset, the magenta line represents the BB segmentation of E_z, and the gray shaded regions indicate periods of negative departures of E_z values from the mean value. The BB and HOP methods also reveal a significant deviation from the mean value in the afternoon of May 10, aligning with the observed deviation from fair-weather conditions, followed by a dip to −31.72 V/m, indicating

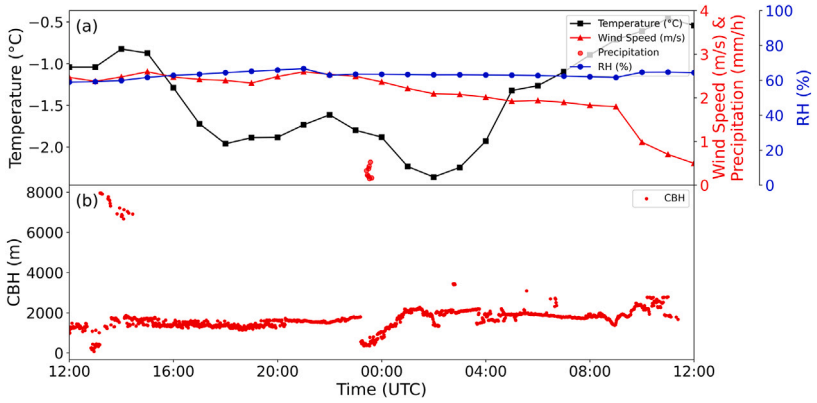

Fig. 3. (a) Meteorological conditions showing temperature, wind speed, relative humidity, and precipitation, and (b) cloud base height (CBH) during May 10–11, 2024.

a statistically significant negative departure from the mean value. After this dip, two significant enhancements above the mean level are observed.

The temperature, wind speed, relative humidity, and precipitation during the study period are shown in Fig. 3(a). CBH is also plotted in Fig. 3(b). The relative humidity is below 67%, and wind speeds remained below 4 m/s. The CBH values remain mostly between 1500–1700 m during the event however, it suddenly drops to very low values at 23:10 UTC on 10th May coinciding with the rapid decrease of Electric field (Fig. 2). It quickly recovers with the increase in electric field and after 00:30 UTC on 11th May, the CBH stays mostly between 1800–2100 m with small variations. During the event NCCS reported no precipitation, but the local optical disdrometer detected very light snowfall for a short period of few minutes during the main phase of the storm from 23:25 UTC to 23:37 UTC on 10th May. Previous studies have also shown that FD events change atmospheric ionization, which in turn affects aerosol and cloud microphysics, as well as cloud cover. Dickinson (1975), Pallé Bagó and Butler (2000). Svensmark et al. (2012) reported the decrease in aerosol and cloud cover during the FD event, suggesting a link between reduced ionization and cloud variability. Using a fair-weather approach in combination with the BB and HOP methods, the three significant departures in the E_z data were identified, including the sharp negative dip and subsequent enhancements observed on May 10–11, 2024.

4.3. Connection between space weather and electric field variation

4.3.1. E_z variations during forbush decrease

The temporal variation of CRI from 12:00 UTC on 10 May to 12:00 UTC on 11 May is shown in Fig. 4(a). To understand the space weather impact on the local electric field, the ground magnetometer data is further explored. In Fig. 4(b), the X-component of magnetic field from three local magnetometer data were shown. Before the arrival of the interplanetary shock on May 10, CRI remained relatively stable, but immediately after the shock at 17:05 UTC on May 10, a gradual decline began (Fig. 4(a)). As the storm progressed, a significant decrease in CRI was observed during the passage of the sheath and complex ejecta regions, reaching a maximum reduction of approximately 15% at 23:26 UTC on May 10 compared to the mean CRI in April 2024. This rapid decrease is due to an increase in solar wind pressure and interplanetary magnetic field disturbances caused by CMEs, leading to a FD (Baral et al., 2023; Kilpua et al., 2017). As the CRI starts to drop, and at the same time, the X-component of nearby ground-based magnetometers began to show a negative bay, marking the onset of an evening polar substorm (Fig. 4(b)).

The initial small decrease in E_z around 17:05 UTC on May 10, as shown on Fig. 4(c), coincides with the arrival of the interplanetary shock at Earth. This short-lived decrease in E_z is quickly followed by a return to positive values. Around 18:00 UTC, E_z shows a positive deviation, whereas the magnetometer X-component continues in its negative bay-like disturbances (Fig. 4(b)), consistent with the ongoing development of the evening substorm (Kleimenova et al., 2025). Subsequently, the magnetic field shifts toward positive values and E_z began to decrease around 22:30 UTC on May 10 and shows a sharp decline, plunging to nearly −44.13 V/m at 23:30 UTC as the CRI reaches its minimum value.

During the period of FD, CBH also dropped to a lower height and light precipitation occurred for few minutes (Fig. 3). The precipitation type was classified as snow based on the SYNOP weather code provided by the optical disdrometer. However, the reduction in E_z began earlier than these meteorological changes. To better understand the influence of snowfall on E_z, precipitation events from the period 2023–2025 were examined. Fig. 5 presents four representative snowfall events, with two cases from nearby dates in the same month as well as two from different months and year to highlight the general trend. The corresponding wind speed and CBH variations are also shown. During all the four events, the wind speed remained below 5 m/s, and low CBH was observed during the time of snowfall. During these events, snowfall resulted in an enhancement of E_z, consistent with earlier studies showing that snow-related charging processes tend to enhance the near-surface electric field (Shumilov et al., 2005; Bennett and Harrison, 2007). To further examine the consistency and variability of this behavior across events, a statistical analysis was performed using all four snowfall cases. The histogram of E_z for all four snow events are shown in Fig. 6. The majority of E_z values were concentrated at low positive ranges and the distribution is positively skewed, with a long tail extending toward higher positive values. During the selected snowfall events, the mean E_z is 954.5 V/m, the median is 546 V/m, and the interquartile range (IQR) is 677.6 V/m, indicating substantial variability in the E_z. This behavior contrasts with the negative deviation observed during the present FD event, indicating that snowfall by itself has opposite impact and may be responsible for short lived nature of the FD induced dip. On the other hand, the simultaneous variation of local magnetic field and electric field points toward the efficient coupling of lower and upper atmosphere during the forbush period. Kleimenova et al. (2008, 2013) also reported the negative deviation in E_z with simultaneous magnetic activity as recorded by ground-based magnetometer observatories during the main phase of the storm. This indicates that the E_z reduction is closely linked with the geomagnetic disturbance and the decrease in CRI.

During the geomagnetic storm, the GCRs are shielded by the sheath and complex ejecta, reducing the number of GCRs that penetrate the Earth's atmosphere. This leads to a decrease in ionization level in the

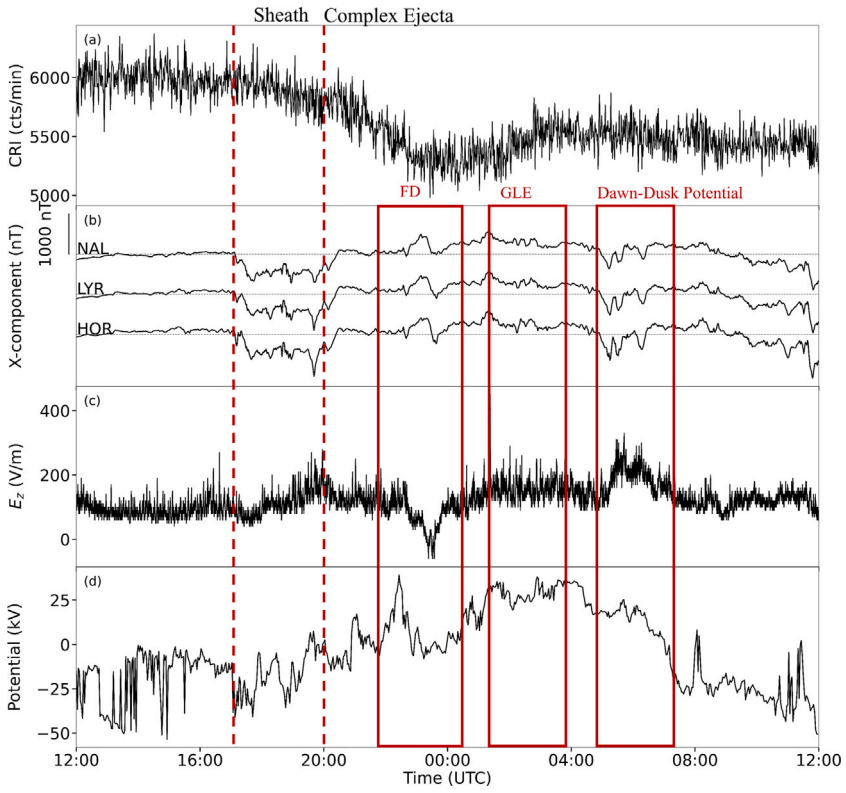

Fig. 4. (a) Temporal variation of CRI obtained from the Oulu Neutron Monitor, and (b) The magnetograms from the selected IMAGE stations (c) The corresponding E_z from Ny-Ålesund station during May 10–11, 2024, (d) The ionospheric potential measured by SuperDARN over Ny-Alesund.

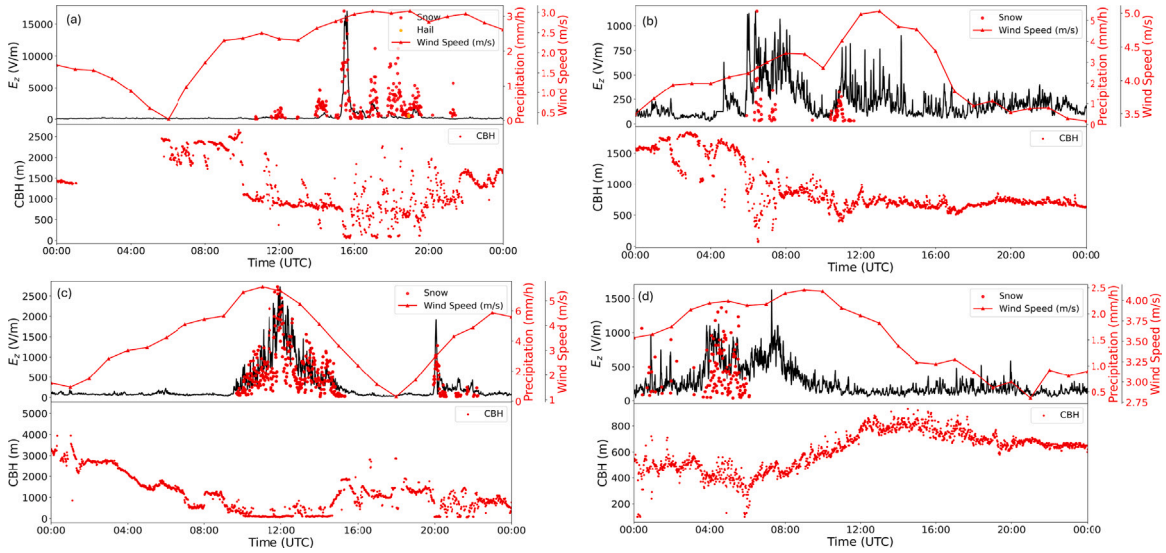

Fig. 5. Variation of E_z during snowfall events: (a) 12 May 2024, (b) 21 May 2024, (c) 14 Jan 2025, (d) 29 April 2025.

atmosphere, which in turn lowers atmospheric conductivity. Several studies suggested that during space weather disturbances like FDs and SPEs, the upward j_z in the GEC is not constant (Herman et al., 1978; Sapkota and Varshneya, 1990; Farrell and Desch, 2002). During the FD, reduced ionization at high latitudes leads decrease in atmospheric conductivity, which in turn may have resulted in a weakening of the j_z and a corresponding reduction in E_z (Li et al., 2023; Li et al., 2024). Such a reduction in E_z during the FD at high and mid latitude stations has also been reported by Marcz (1997), Li et al. (2023). In contrast (Fu et al., 2025) observed the increase in E_z values during the FD phase for mid-latitude station.

4.3.2. E_z variations during GLE

The GLE event was also observed during the recovery phase on May 11, 2024, starting around 01:30 UTC and peaking at 03:00 UTC. It was observed that around 1:30 UTC, the E_z values increased significantly above the fair-weather condition during the time of the GLE, with values fluctuating roughly between 140 V/m and 220 V/m and then gradually decreasing (Fig. 2(a)). During GLE, the high-energy particles penetrate the lower atmosphere, which increases the conductivity. It is known that E_z and j_z of the GEC are controlled by the column resistance, which is strongly influenced by SEPs that can penetrate

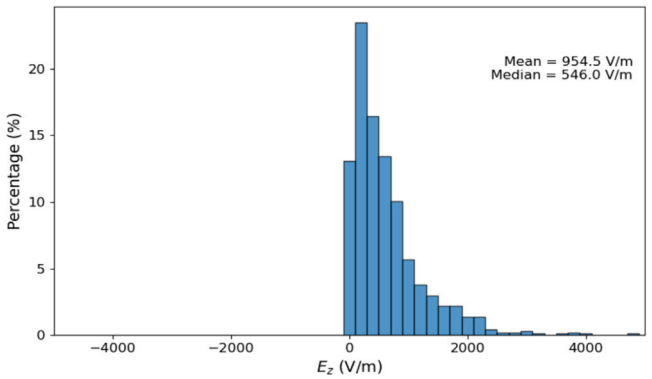

Fig. 6. Combined histogram showing the distribution of E_z during four snowfall events: 12 May 2024, 21 May 2024, 14 January 2025, and 29 April 2025.

the lower atmosphere (Holzworth et al., 1987). As proposed by Farrell and Desch (2002), Markson (1978) during SEPs, the ionization rate increases above a certain height and enhances the atmospheric conductivity. This reduces the resistance between the atmosphere and the ionosphere, allowing more upward current to flow through the GEC. This leads to increased charge accumulation near the ionospheric boundary of the GEC, which in turn enhances the E_z observed at the surface. An increase in E_z in the middle atmosphere during a GLE event has also been reported by other researchers (Zadorozhny et al., 1994; Zadorozhny and Tyutin, 1998; Holzworth et al., 1987). They showed that the increase in E_z during GLE is only possible when there is a faster increase in the aerosol concentration than in the conductivity. Furthermore, Tacza et al. (2018) reported a 3-hour decrease in E_z during cosmic ray enhancement, followed by an increase that occurred approximately 7 h after the onset of the SPE. They suggested that this increase may be attributed to the SPE/GLE that occurred on 17 May 2012 (GLE#71). In contrast, Fu et al. (2025) reported a contrasting response during the GLE, observing a brief decrease in E_z.

4.3.3. Dawn–dusk potential effects on E_z

Another prominent rise in the E_z starts around 05:00 UTC on May 11 and reaches a maximum value of 302 V/m, marking a significant deviation from the fair-weather electric field conditions before gradually decreasing by 07:00 UTC (Fig. 4(c)). Around the same time, the X-component of the ground-based magnetic field (Fig. 4(b)) exhibits a negative magnetic bay, indicating the enhanced geomagnetic activity that coincides with the observed increase in E_z. Previous studies have shown that variations in E_z can also result from the mapping of horizontal ionospheric electric fields down to the Earth's surface, caused by the dawn–dusk electric potential difference generated by the interaction between solar wind and the Earth's magnetosphere. The connection between the ionospheric potential and ground-level electric field has been reported in both the Northern and Southern Hemispheres. For example, in the Southern Hemisphere, this link has been observed at Vostok Station (Frank-Kamenetsky et al., 1999; Burns et al., 2005; Victor et al., 2016) and Maitri Station (Victor et al., 2016; Panneerselvam et al., 2010; Siingh et al., 2013). In the Northern Hemisphere, similar observations have been made at Hornsund (Odzimek et al., 2011; Frank-Kamenetskii et al., 2012).

To assess this impact, the temporal variation of the ionospheric electric potential measured by SuperDARN over Ny-Ålesund is shown in Fig. 4(d). SuperDARN is a global network of high-frequency radars to study the plasma flow in the polar ionosphere (Greenwald et al., 1995). It provides a valuable representation of the dawn–dusk potential across the polar region, which plays a significant role in modulating the ionospheric potential and atmospheric electrical conditions. During the afternoon hours of 10 May (around 12:00–18:00 UTC), corresponding to a magnetically quiet period, the ionospheric electric potential remains predominantly negative, while E_z exhibits relatively steady behavior with minor fluctuations. From 18:00 to 22:00 UTC, E_z closely follows the overall temporal pattern of the ionospheric electric potential. Around 22:30 UTC, a reduction in the ionospheric potential is observed, and a corresponding brief decrease in E_z occurs during the same period. Subsequently, in the early hours of 11 May, both the ionospheric electric potential and E_z show a enhancement.

It is also necessary to examine the spatial distribution of the ionospheric electric potential. To examine the enhancement in E_Z around 5:00 UTC to 7:00 UTC, the ionospheric convection patterns observed by SuperDARN are used. Furthermore, the Cross Polar Cap Potential (CPCP), defined as the potential difference across the polar cap, indicates the overall convection strength and helps explain variations in the ionospheric electric field that can affect E_z measurements. As reported by Li et al. (2024), the positive or negative deviation in E_z also depends on the station's position relative to the plasma convection cell. Convection maps for four time intervals, Fig. 7(a) during the period of relatively low geomagnetic activity on May 10 (14:40–14:42 UTC), when the Kp index was 3, Fig. 7(b,c,d) during the disturbed period on May 10 (17:30–17:32), May 11 (05:30–05:32 UTC), and on May 11 (07:30–07:32 UTC) are shown with a red star depicting the station location. The black color outer boundary indicates the auroral oval (Imber et al., 2013).

During all times, the study station is within the auroral oval as shown in Fig. 7. In Fig. 7(a), during the magnetic quiet period, the CPCP is 30 kV, whereas during the disturbed period, the CPCP reaches the value of 110 kV on May 10 (17:30–17:32 UTC) and the station is under negative convection cell. After this interval, the station is observed under both negative and positive convection cells during different times. This period also corresponds to the FD phase, during which the ionospheric convection pattern is highly variable. From May 11, the station begins to be located under the positive convection cell. As shown in the convection map at 05:30–05:32 UTC, where the station lies within the positive cell and the CPCP difference is about 52 kV. The corresponding E_z values show positive deviation (05:30–05:32 UTC) more than the fair-weather conditions. This high potential difference is mapped down to the Earth's surface along the magnetic field lines and is coupled with the E_z, leading to its enhancement. After this enhancement, the station is under to the negative convection cell (07:30–07:32 UTC) with value of 114 kV and the E_z values decrease and lie within the fair-weather range shown in the Fig. 4(c). These results agree with the findings of Victor et al. (2015), Tinsley et al. (1998), Kleimenova et al. (2018).

To further strengthen the interpretation, the ionospheric electric potential patterns derived from SuperDARN for four selected time periods are compared with the Weimer model outputs (Weimer, 2005) corresponding to the same or the nearest available time intervals (Fig. 8). The Weimer model estimates high-latitude ionospheric electric potentials using solar wind and IMF parameters. By examining the corresponding Weimer potential maps for these periods, we assess whether the timing and magnitude of modeled electrodynamic variations due to space-weather are consistent with the SuperDARN results and the observed E_z response. The convection cell pattern observed from SuperDARN and weimer model are well matched supporting the linkage between large-scale space-weather electrodynamics and surface E_z variations. Sabri et al. (2025) also compared the Weimer model with SuperDARN observations for the May 2024 geomagnetic storm and show that the timing and overall pattern of the CPCP during quiet and disturbed periods are generally consistent between the model and observations. Although differences in CPCP magnitude were found mainly because SuperDARN can underestimate CPCP during strong geomagnetic activity, even though the timing and overall trend are consistent with the model.

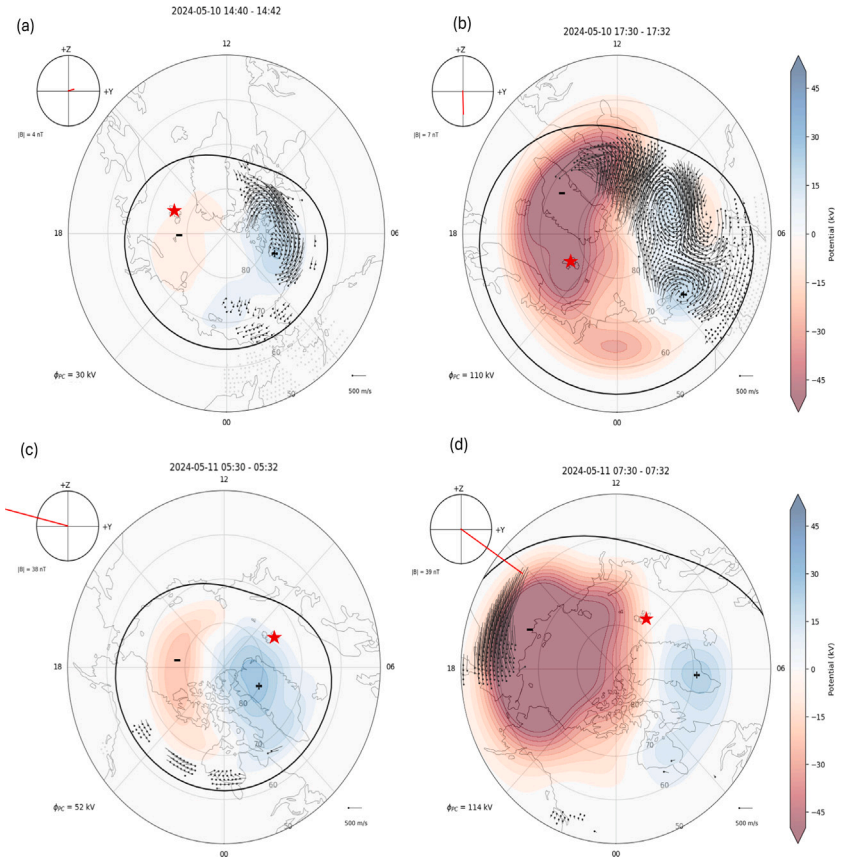

Fig. 7. Convection maps for four time intervals: (a) during the period of relatively low geomagnetic activity on May 10 (14:40–14:42 UTC), when the Kp index was 3, and (b-d) during the disturbed period on May 10 (17:30–17:32), May 11 (05:30–05:32 UTC), and on May 11 (07:30–07:32 UTC). The positive and negative potential cells in the convection maps are indicated by blue and red colors, respectively. Arrows represent plasma convection velocity, and the CPCP value and IMF orientation are provided for the respective time intervals.

5. Summary and conclusions

This study investigates the variation in the E_z during the strong geomagnetic storm of May 2024 in the Arctic region. Understanding how space weather influences the atmospheric electric field is crucial, as it impacts the GEC, cloud physics, and weather dynamics. While prior studies have investigated this interaction, their findings remain inconsistent. The rare and powerful G5-class geomagnetic storm of May 2024, accompanied by the simultaneous occurrence of a FD and a GLE, provides an opportunity to study how space weather events influence the atmospheric electric field in the high-latitude Arctic region.

In this study, three major pathways are identified through which the storm affected the atmospheric electric field: FD, GLE, and dawn–dusk ionospheric potential variations. During the main phase of the storm and the associated FD, E_z is observed to decrease rapidly coinciding with the lowest CRI timing and clear disturbances in the X-component of the geomagnetic field. Usually, the reduced flux of GCRs lowers the atmospheric conductivity and increases the E_z, assuming j_z is constant. The present findings indicate that j_z may also have decreased, leading to a decrease in E_z. Light snowfall was also noticed for a few minutes along with reduced CBH coinciding this period which explains the short lived nature of the dip as snowfall usually associated with increase in E_z. The decrease in E_z began earlier than these meteorological changes and the simultaneous rapid negative deviation in E_z along with the minimum CRI and enhanced magnetic disturbance indicate the efficient coupling of lower and upper atmosphere during the FD.

In contrast, during the recovery phase, an increase in the E_z has been observed. This can be explained if the j_z increases or the conductivity decreases. An increased atmospheric ionization due to the influx of SEPs can reduce the column resistance between the atmosphere and ionosphere, leading to enhanced upward current. Moreover, reduction of conductivity can also be possible if the aerosol concentration increases faster than the conductivity and the ejection of positive charges in the polar atmosphere (Tonev, 2024). A further enhancement in E_z during the early morning hours of May 11 was also observed coinciding with intensified magnetic disturbance observed in magnetometer and a increase in the dawn–dusk ionospheric potential difference. The comparison between quiet and disturbed periods using SuperDARN convection maps, which is in good agreement with consistent with the output of weimer model, shows that a larger horizontal ionospheric potential is mapped along magnetic field lines to the ground, resulting in a positive deviation in E_z.

The present study indicates a complex interaction between the upper and lower atmosphere in the presence of different physical processes involved, the observation location, and the magnetic storm's intensity. The variation in E_z is expected to reflect latitude-dependent electrodynamic processes. At high latitudes, the atmospheric electric field is more strongly influenced by changes in ionospheric potential associated with polar cap convection and magnetosphere-ionosphere coupling. In contrast, at mid-latitudes, variations in Ez are more likely governed by changes in columnar resistance and local conductivity modulated by meteorological processes. Therefore, differences between the observations may arise from both latitude dependence and differing

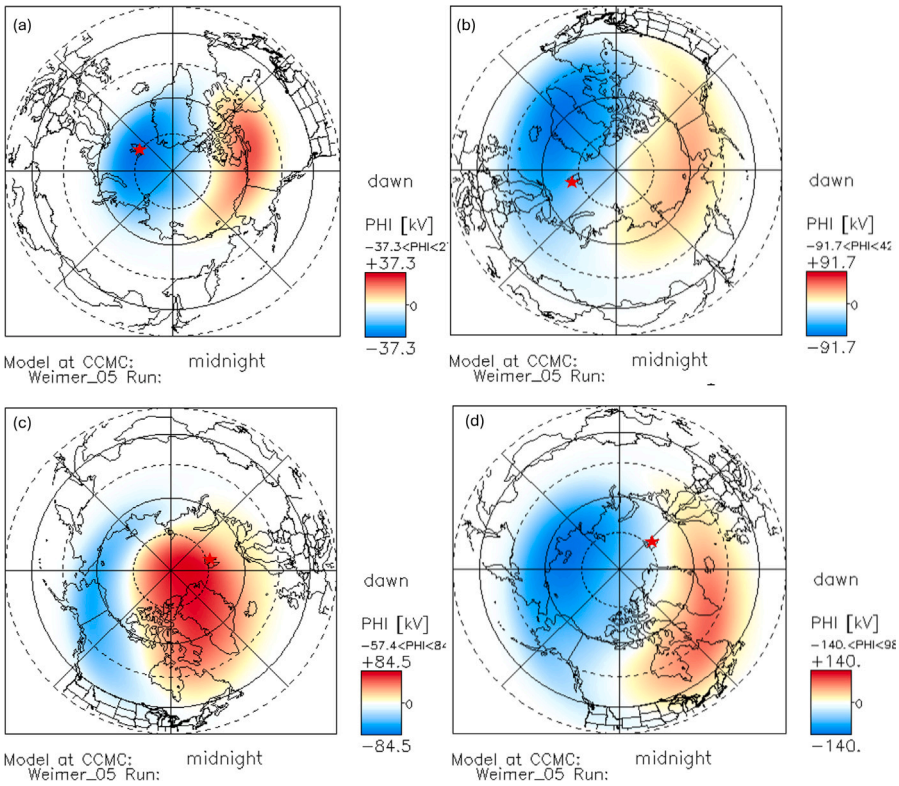

Fig. 8. Weimer model convection patterns corresponding to the same four time intervals selected for the SuperDARN maps: (a) 10 May (14:40 UTC; Kp = 3, relatively quiet conditions) and (b-d) disturbed periods on 10 May (17:37 UTC), 11 May (05:32 UTC), and 11 May (07:28 UTC). The positive and negative potential cells in the convection maps are indicated by red and blue colors, respectively.

sensitivities to ionospheric potential variations. To better understand the impact of geomagnetic storms on the GEC, further studies are needed to explore these complex interactions between space weather and atmospheric electric fields, especially in high-latitude regions.

CRediT authorship contribution statement

Kavita: Writing – original draft, Methodology, Investigation. **Saurabh Das:** Writing – review & editing, Supervision, Conceptualization. **Nuncio Murukesh:** Supervision.

Declaration of competing interest

The authors declare that they have no known competing financial interests or personal relationships that could have appeared to influence the work reported in this paper.

Acknowledgments

The authors gratefully acknowledge the Ministry of Earth Sciences, Government of India, and the Director, ESSO-NCPOR, for their continued support throughout the study (Project no. RIS 12301 and Contribution number is J-90/2025-26). The authors also acknowledge the teams for providing SuperDARN data, IMAGE Magnetometer Array data, ECMWF ERA5 reanalysis data and NASA's OMNI space weather data.

Data availability

The Space weather parameters were obtained from the OMNI web interface of NASA http://omniweb.gsfc.nasa.gov and CRI data from the OULU neutron monitor https://cosmicrays.oulu.fi/. The SuperDARN data were obtained from https://superdarn.ca/. The Weimer model output were taken from https://ccmc.gsfc.nasa.gov/. The magnetometer data were obtained from https://space.fmi.fi/image/www/index.php?. The data of E_z for Ny-Ålesund, Artic is available at https://data.ncpor.res.in/newhtml/3.

References

Araki, T., 1977. Global structure of geomagnetic sudden commencements. Planet. Space Sci. 25 (4), 373–384. http://dx.doi.org/10.1016/0032-0633(77)90053-8.

Baral, R., Adhikari, B., Calabia, A., Shah, M., Mishra, R.K., Silwal, A., Bohara, S., Manandhar, R., del Peral, L., Frías, M.D.R., 2023. Spectral features of forbush decreases during geomagnetic storms. J. Atmos. Sol.-Terr. Phys. 242, 105981. http://dx.doi.org/10.2139/ssrn.4051359.

Bennett, A., Harrison, R., 2007. Atmospheric electricity in different weather conditions. Weather 62 (10), 277–283. http://dx.doi.org/10.1002/wea.97.

Blasi, P., 2013. The origin of galactic cosmic rays. Astron. Astrophys. Rev. 21, 1–73. http://dx.doi.org/10.1016/j.nima.2008.01.036.

Burlaga, L., Plunkett, S., St. Cyr, O., 2002. Successive CMEs and complex ejecta. J. Geophys. Res.: Space Phys. 107 (A10), SSH–1. http://dx.doi.org/10.1029/2001JA000255.

Burlaga, L., Sittler, E., Mariani, F., Schwenn, a.R., 1981. Magnetic loop behind an interplanetary shock: Voyager, Helios, and IMP 8 observations. J. Geophys. Res.: Space Phys. 86 (A8), 6673–6684. http://dx.doi.org/10.1029/JA086iA08p06673.

Burns, G., Frank-Kamenetsky, A., Troshichev, O., Bering, E., Reddell, B., 2005. Interannual consistency of bi-monthly differences in diurnal variations of the ground-level, vertical electric field. J. Geophys. Res.: Atmospheres 110 (D10), http://dx.doi.org/10.1029/2004JD005469.

Chauhan, M., Shrivastava, S., Richharia, M., Jain, M., Jain, A., 2008. Study of two major forbush decrease events of 2005. In: Proceedings of the 30th International Cosmic Ray Conference, Mexico City, vol. 1, p. 307.

Crosby, N., Mavromichalaki, H., Malandraki, O., Gerontidou, M., Karavolos, M., Lingri, D., Makrantoni, P., Papailiou, M., Paschalis, P., Tezari, A., 2024. Very high energy solar energetic particle events and ground level enhancement events: Forecasting and alerts. Space Weather. 22 (9), e2023SW003839. http://dx.doi.org/10.1029/2023SW003839.

Dickinson, R.E., 1975. Solar variability and the lower atmosphere. Bull. Am. Meteorol. Soc. 56 (12), 1240–1248. http://dx.doi.org/10.1175/1520-0477(1975)056<1240:SVATLA>2.0.CO;2.

Eisenstein, D.J., Hut, P., 1998. HOP: a new group-finding algorithm for N-body simulations. Astrophys. J. 498 (1), 137. http://dx.doi.org/10.1086/305535.
Engfer, D.W., Tinsley, B.A., 1999. An investigation of short-term solar wind modulation of atmospheric electricity at mauna loa observatory. J. Atmos. Sol.-Terr. Phys. 61 (13), 943–953. http://dx.doi.org/10.1016/S1364-6826(99)00057-7.
Farrell, W., Desch, M., 2002. Solar proton events and the fair weather electric field at ground. Geophys. Res. Lett. 29 (9), 1–37. http://dx.doi.org/10.1029/2001GL013908.
Frank-Kamenetskii, A., Kotikov, A., Kruglov, A., Burns, G., Kleimenova, N., Kozyreva, O., Kubitski, M., Odzimek, A., 2012. Variations in the near-surface atmospheric electric field at high latitudes and ionospheric potential during geomagnetic perturbations. Geomagn. Aeron. 52 (5), 629–638. http://dx.doi.org/10.1134/S0016793212050064.
Frank-Kamenetsky, A., Burns, G., Troshichev, O., Papitashvili, V., Bering, E., French, W., 1999. The geoelectric field at vostok, antarctica: its relation to the interplanetary magnetic field and the cross polar cap potential difference. J. Atmos. Sol.-Terr. Phys. 61 (18), 1347–1356. http://dx.doi.org/10.1016/S1364-6826(99)00089-9.
Fu, S., Li, G., Tacza, J., Chen, T., Peng, J., 2025. Global electric circuit response to the may 2024 geospace superstorm from China's Gar station observation. Phys. Fluids 37 (11), http://dx.doi.org/10.1063/5.0292958.
Gonzalez-Esparza, J.A., Sanchez-Garcia, E., Sergeeva, M., Corona-Romero, P., Gonzalez-Mendez, L., Valdes-Galicia, J., Aguilar-Rodriguez, E., Rodriguez-Martinez, M., Ramirez-Pacheco, C., Castellanos, C., et al., 2024. The mother's day geomagnetic storm on 10 May 2024: Aurora observations and low latitude space weather effects in Mexico. Space Weather. 22 (11), e2024SW004111. http://dx.doi.org/10.1029/2024SW004111.
Greenwald, R., Baker, K., Dudeney, J., Pinnock, M., Jones, T., Thomas, E., Villain, J.P., Cerisier, J.C., Senior, C., Hanuise, C., et al., 1995. DARN/SuperDARN: a global view of the dynamics of high-latitude convection. Space Sci. Rev. 71, 761–796. http://dx.doi.org/10.1007/BF00751350.
Hajra, R., Tsurutani, B.T., Lakhina, G.S., Lu, Q., Du, A., 2024. Interplanetary causes and impacts of the 2024 May superstorm on the geosphere: An overview. Astrophys. J. 974 (2), 264. http://dx.doi.org/10.3847/1538-4357/ad7462.
Harrison, R., Nicoll, K., 2018. Fair weather criteria for atmospheric electricity measurements. J. Atmos. Sol.-Terr. Phys. 179, 239–250.
Hayakawa, H., Ebihara, Y., Mishev, A., Koldobskiy, S., Kusano, K., Bechet, S., Yashiro, S., Iwai, K., Shinbori, A., Mursula, K., et al., 2025. The solar and geomagnetic storms in 2024 May: A flash data report. Astrophys. J. 979 (1), 49. http://dx.doi.org/10.3847/1538-4357/ad9335.
Herman, J.R., Goldberg, R.A., Goldberg, R.A., 1978. Sun, Weather, and Climate, vol. 426, Scientific and Technical Information Office, National Aeronautics and Space Administration..
Holzworth, R., Norville, K., Williamson, P., 1987. Solar flare perturbations in stratospheric current systems. Geophys. Res. Lett. 14 (8), 852–855. http://dx.doi.org/10.1029/GL014i008p00852.
Imber, S.M., Milan, S., Lester, M., 2013. The heppner-maynard boundary measured by SuperDARN as a proxy for the latitude of the auroral oval. J. Geophys. Res.: Space Phys. 118 (2), 685–697. http://dx.doi.org/10.1029/2012JA018222.
Kilpua, E., Koskinen, H.E., Pulkkinen, T.I., 2017. Coronal mass ejections and their sheath regions in interplanetary space. Living Rev. Sol. Phys. 14, 1–83. http://dx.doi.org/10.1007/s41116-017-0009-6.
Kleimenova, N., Gromova, L., Gromov, S., Malysheva, L., 2025. Ground-based geomagnetic disturbances and Pi2 pulsations in the main phase of the superstorm on May 10, 2024. Adv. Space Res. http://dx.doi.org/10.1016/j.asr.2025.04.025.
Kleimenova, N., Kozyreva, O., Kubicki, M., Michnowski, S., 2011. Substorm effects in the polar latitude atmospheric electric field disturbances. Phys. Auror. Phenom. 33 (1), 167–170.
Kleimenova, N., Kozyreva, O., Michnowski, S., Kubicki, M., 2008. Effect of magnetic storms in variations in the atmospheric electric field at midlatitudes. Geomagn. Aeron. 48, 622–630. http://dx.doi.org/10.1134/S0016793208050071.
Kleimenova, N., Kozyreva, O., Michnowski, S., Kubicki, M., 2013. Influence of geomagnetic disturbances on atmospheric electric field (Ez) variations at high and middle latitudes. J. Atmos. Sol.-Terr. Phys. 99, 117–122. http://dx.doi.org/10.1016/j.jastp.2012.07.009.
Kleimenova, N., Kubicki, M., Odzimek, A., Malysheva, L., Gromova, L., 2017. Effects of geomagnetic disturbances in daytime variations of the atmospheric electric field in polar regions. Geomagn. Aeron. 57, 266–273. http://dx.doi.org/10.1134/S0016793217030070.
Kleimenova, N., Odzimek, A., Michnowski, S., Kubicki, M., 2018. Geomagnetic storms and substorms as space weather influence on atmospheric electric field variations. Sun Geosph. 13 (1), 101–107. http://dx.doi.org/10.31401/SunGeo.2018.01.14.
Kumar, C.A., Panneerselvam, C., Nair, K., Jeyakumar, H.J., Selvaraj, C., Gurubaran, S., Venugopal, C., 2009. Apposite of atmospheric electric parameters with the energy coupling function (ε) during geomagnetic storms at high latitude. Atmos. Res. 91 (2–4), 201–205. http://dx.doi.org/10.1016/j.atmosres.2008.06.005.
Li, L., Chen, T., Shen, C., Ti, S., Wang, S., Cai, C., Li, W., Luo, J., 2023. Near-surface atmospheric electric field changes through magnetic clouds via coronal mass ejections. Geosci. Lett. 10 (1), 45. http://dx.doi.org/10.1186/s40562-023-00299-2.
Li, W., Sun, Z., Chen, T., Yan, Z., Luo, J., Xu, Q., Ma, Z., 2024. Different effects of a super storm on atmospheric electric fields at different latitudes. Atmosphere 15, 1314. http://dx.doi.org/10.3390/atmos15111314.
Li, R., Ti, S., Li, L., Song, J., Chen, T., 2025. Diurnal variations of atmospheric electric fields on fair weather days and its correlations with aerosols, wind speed, irradiance, and relative humidity. Sci. Rep. 15, http://dx.doi.org/10.1038/s41598-025-89788-2.
Liu, Y.D., Hu, H., Zhao, X., Chen, C., Wang, R., 2024. A pileup of coronal mass ejections produced the largest geomagnetic storm in two decades. Astrophys. J. Lett. 974 (1), L8. http://dx.doi.org/10.3847/2041-8213/ad7ba4.
Mallios, S.A., Papaioannou, A., Herbst, K., Papangelis, G., Hloupis, G., 2022. Study of the ground level enhancements effect on atmospheric electric properties and mineral dust particle charging. J. Atmos. Sol.-Terr. Phys. 233, 105871. http://dx.doi.org/10.1016/j.jastp.2022.105871.
Marcz, F., 1997. Short-term changes in atmospheric electricity associated with forbush decreases. J. Atmos. Sol.-Terr. Phys. 59 (9), 975–982. http://dx.doi.org/10.1016/S1364-6826(96)00076-4.
Markson, R., 1978. Solar modulation of atmospheric electrification and possible implications for the sun–weather relationship. Nature 273 (5658), 103–109. http://dx.doi.org/10.1038/273103a0.
Marshall, T.C., Rust, W.D., Stolzenburg, M., Roeder, W.P., Krehbiel, P.R., 1999. A study of enhanced fair-weather electric fields occurring soon after sunrise. J. Geophys. Res.: Atmospheres 104 (D20), 24455–24469. http://dx.doi.org/10.1029/1999JD900418.
Meyer, M., Scargle, J.D., Blandford, R.D., 2019. Characterizing the gamma-ray variability of the brightest flat spectrum radio quasars observed with the Fermi LAT. Astrophys. J. 877 (1), 39. http://dx.doi.org/10.3847/1538-4357/ab1651.
Michnowski, S., Odzimek, A., Kleimenova, N., Kozyreva, O., Kubicki, M., Klos, Z., Israelsson, S., Nikiforova, N., 2021. Review of relationships between solar wind and ground-level atmospheric electricity: Case studies from Hornsund, Spitsbergen, and Swider, Poland. Surv. Geophys. 42 (3), 757–801. http://dx.doi.org/10.1007/s10712-021-09639-3.
Michnowski, S., Odzimek, A., Kleimenova, N., Kozyreva, O., Kubicki, M., Nikiforova, N., 2014. Review of examples of solar wind lower atmosphere coupling observed in the electric field (Ez) variations at the earth's surface during magnetic storms. In: Proceedings of the 15th International Conference on Atmospheric Electricity. pp. 21–26.
Odzimek, A., Kubicki, M., Lester, M., Grocott, A., 2011. Relation between superdarn ionospheric potential and ground electric field at polar station hornsund. In: Proc. 14th Int. Conference on Atmospheric Electricity.
Pallé Bagó, E., Butler, C., 2000. The influence of cosmic rays on terrestrial clouds and global warming. Astron. Geophys. 41 (4), 4–18. http://dx.doi.org/10.1046/j.1468-4004.2000.00418.x.
Panneerselvam, C., Anil Kumar, C., Dhar, A., Nair, K., Selvaraj, C., Gurubaran, S., Pathan, B., 2010. Instrumentation for the surface measurements of atmospheric electrical parameters at Maitri, Antarctica: First results. Earth, Planets Space 62 (6), 545–549. http://dx.doi.org/10.5047/eps.2010.06.001.
Papitashvili, V., Belov, B., Faermark, D., Feldstein, Y.I., Golyshev, S., Gromova, L., Levitin, A., 1994. Electric potential patterns in the northern and southern polar regions parameterized by the interplanetary magnetic field. J. Geophys. Res.: Space Phys. 99 (A7), 13251–13262. http://dx.doi.org/10.1029/94JA00822.
Park, C., 1976. Downward mapping of high-latitude ionospheric electric fields to the ground. J. Geophys. Res. 81 (1), 168–174. http://dx.doi.org/10.1029/JA081i001p00168.
Potdar, S.S., Siingh, D., 2024. The atmospheric global electric circuit: A review. J. Indian Geophys. Uni 28 (4), 247–267.
Reagan, J., Meyerott, R., Evans, J., Imhof, W., Joiner, R., 1983. The effects of energetic particle precipitation on the atmospheric electric circuit. J. Geophys. Res.: Ocean. 88 (C6), 3869–3878. http://dx.doi.org/10.1029/JC088iC06p03869.
Reddell, B., Benbrook, J., Bering, E., Cleary, E., Few, A., 2004. Seasonal variations of atmospheric electricity measured at Amundsen-Scott south pole station. J. Geophys. Res.: Space Phys. 109 (A9), http://dx.doi.org/10.1029/2004JA010536.
Roble, R., Hays, P., 1979. A quasi-static model of global atmospheric electricity 2. Electrical coupling between the upper and lower atmosphere. J. Geophys. Res.: Space Phys. 84 (A12), 7247–7256. http://dx.doi.org/10.1029/JA084iA12p07247.
Rycroft, M.J., Harrison, R.G., Nicoll, K.A., Mareev, E.A., 2008. An overview of earth's global electric circuit and atmospheric conductivity. Planet. Atmospheric Electr. 83–105. http://dx.doi.org/10.1007/s11214-008-9368-6.
Sabri, S., Mahmoudian, A., Poedts, S., 2025. Investigation of the may 2024 solar storm through EUHFORIA/gorgon-space simulations and global superdarn observations. J. Geophys. Res.: Space Phys. 130 (11), e2024JA033554. http://dx.doi.org/10.1029/2024JA033554.
Sapkota, B., Varshneya, N., 1990. On the global atmospheric electrical circuit. J. Atmos. Terr. Phys. 52 (1), 1–20. http://dx.doi.org/10.1016/0021-9169(90)90110-9.
Shumilov, O., Kasatkina, E., Frank-Kamenetsky, A., 2015. Effects of extraordinary solar cosmic ray events on variations in the atmospheric electric field at high latitudes. Geomagn. Aeron. 55, 650–657. http://dx.doi.org/10.1134/S0016793215050151.
Shumilov, O., Kasatkina, E., Kulichkov, S., Kallistratova, M., Vasil'ev, A., 2005. Meteorological effects in the atmospheric electric field in the high latitudes. Izvestiia-Russian Academy Sciences Atmospheric Oceanic Physics C/C Izvestiia-Rossiiskaia Akademiia Nauk Fizika Atmosfery I Okeana 41 (5), 555.
Siingh, D., Singh, R., 2010. The role of cosmic rays in the Earth's atmospheric processes. Pramana 74, 153–168.

Siingh, D., Singh, R., Gopalakrishnan, V., Selvaraj, C., Panneerselvam, C., 2013. Fair-weather atmospheric electricity study at maitri (Antarctica). Earth, Planets Space 65 (12), 1541–1553. http://dx.doi.org/10.5047/eps.2013.09.011.

Smirnov, S., 2014. Reaction of electric and meteorological states of the near-ground atmosphere during a geomagnetic storm on 5 april 2010. Earth, Planets Space 66, 1–8. http://dx.doi.org/10.1186/s40623-014-0154-2.

Souvatzoglou, G., Papaioannou, A., Mavromichalaki, H., Dimitroulakos, J., Sarlanis, C., 2014. Optimizing the real-time ground level enhancement alert system based on neutron monitor measurements: Introducing GLE alert plus. Space Weather. 12 (11), 633–649. http://dx.doi.org/10.1002/2014SW001102.

Svensmark, J., Enghoff, M., Svensmark, H., 2012. Effects of cosmic ray decreases on cloud microphysics. Atmospheric Chem. Phys. Discuss. 12 (2), 3595–3617. http://dx.doi.org/10.5194/acpd-12-3595-2012.

Tacza, J., Odzimek, A., Tueros Cuadros, E., Raulin, J.-P., Kubicki, M., Fernandez, G., Marun, A., 2022. Investigating effects of solar proton events and forbush decreases on ground-level potential gradient recorded at middle and low latitudes and different altitudes. Space Weather. 20 (3), e2021SW002944. http://dx.doi.org/10.1029/2021SW002944.

Tacza, J., Raulin, J.P., Mendonca, R., Makhmutov, V., Marun, A., Fernandez, G., 2018. Solar effects on the atmospheric electric field during 2010–2015 at low latitudes. J. Geophys. Res.: Atmospheres 123 (21), 11–970. http://dx.doi.org/10.1029/2018JD029121.

Tinsley, B., Liu, W., Rohrbaugh, R., Kirkland, M., 1998. South pole electric field responses to overhead ionospheric convection. J. Geophys. Res.: Atmospheres 103 (D20), 26137–26146. http://dx.doi.org/10.1029/98JD02646.

Tonev, P., 2024. Hypothetic Explanation of Peculiar Atmospheric Electric Response to SEP at High Latitudes. Experimental Evidence.. In: Sixteenth Workshop on Solar Influences on the Magnetosphere, Ionosphere, and Atmosphere. p. 94. http://dx.doi.org/10.48550/arXiv.2301.12345.

Tulasiram, S., Veenadhari, B., Dimri, A.P., Bulusu, J., Bagiya, M., Gurubaran, S., Parihar, N., Bhanu, R., Seemala, G., Singh, R., Sripathi, S., Singh, S., Vichare, G., 2024. Super-intense geomagnetic storm on 10–11 May 2024: Possible mechanisms and impacts. Space Weather. 22, http://dx.doi.org/10.1029/2024SW004126.

Victor, N.J., Manu, S., Frank-Kamenetsky, A., Panneerselvam, C., Anil Kumar, C., Elango, P., 2016. Network of observations on the atmospheric electrical parameters during geomagnetic storm on 5 April 2010. J. Geophys. Res.: Space Phys. 121 (3), 2407–2417. http://dx.doi.org/10.1002/2015JA022080.

Victor, N.J., Panneerselvam, C., Anil Kumar, C., 2015. Variation of surface electric field during geomagnetic disturbed period at Maitri, Antarctica. J. Earth Syst. Sci. 124 (8), 1721–1733. http://dx.doi.org/10.1007/s12040-015-0638-x.

Weimer, D., 2005. Improved ionospheric electrodynamic models and application to calculating Joule heating rates. J. Geophys. Res.: Space Phys. 110 (A5), http://dx.doi.org/10.1029/2004JA010884.

Wilson, C.T.R., 1921. III. Investigations on lighting discharges and on the electric field of thunderstorms. Philos. Trans. R. Soc. Lond. Ser. A, Contain. Pap. A Math. Or Phys. Character 221 (582–593), 73–115.

Zadorozhny, A., Kikhtenko, V., Kokin, G., Tuchkov, G., Tyutin, A., Chizhov, A., Shtirkov, O., 1994. Middle atmosphere response to the solar proton events of October 1989 using the results of rocket measurements. J. Geophys. Res.: Atmospheres 99 (D10), 21059–21069. http://dx.doi.org/10.1029/93JD03194.

Zadorozhny, A., Tyutin, A., 1998. Effects of geomagnetic activity on the mesospheric electric fields. In: Annales Geophysicae, vol. 16, (12), Springer Verlag Göttingen, Germany, pp. 1544–1551. http://dx.doi.org/10.1007/s00585-998-1544-1.